CHAPTER 7

SWIFT HEAVY ION IRRADIATION OF REDUCED GRAPHENE OXIDE-POLYANILINE NANOTUBES NANOCOMPOSITE ELECTRODE SYSTEM

This chapter deals with the swift heavy ion irradiation effects on the properties of 40 wt. % reduced graphene oxide-polyaniline nanotubes nanocomposite irradiated with 85 MeV C^{6+} ions with different fluences. The morphology and structure of the pristine and irradiated nanocomposites have been studied by HRTEM, XRD, FTIR and micro-Raman spectroscopy. Irradiation induced modifications in thermal and electrical properties of the nanocomposite have been investigated by thermogravimetric analysis, current-voltage and conductivity measurements. BET specific surface area and surface wettability of the pristine and irradiated nanocomposite electrodes have been determined. The electrochemical performance of the nanocomposite before and after irradiation has been investigated in terms of specific capacitance, coulombic efficiency, energy density, power density and cycle life by cyclic voltammetry and galvanostatic charge-discharge measurements. The equivalent series and charge transfer resistances of the electrode and electrolyte have been evaluated using electrochemical impedance spectroscopy.

7.1 Introduction

Owing to the high fluctuations in energy generation and supply from renewable energy sources, electrochemical capacitors, also known as supercapacitors have recently gained an increasing demand due to its high power density, long cycle life and high electrochemical reversibility [351]. Supercapacitors store charge through two mechanisms that are classified as electric double layer capacitance (EDLC) and pseudocapacitance. EDLCs are characterized by a high specific power and cycle life [352], which are generally exhibited by carbon-based materials like carbon nanotubes, activated carbons, graphene etc. Pseudocapacitors use redox-active

materials as electrodes like transition metal oxides and conducting polymers [353] and have higher specific capacitance and energy density than that of EDL capacitors [354]. However, supercapacitors still are unable to replace batteries in energy storage devices due to their lower energy density and specific capacitance. Significant research efforts have been made in combining both pseudocapacitive and EDLC materials to form nanocomposites with high energy density and specific capacitance without loss in power density and cycle life [355, 356]. Recently, conducting polymers have been hybridized with different carbon materials like carbon nanotubes [328], activated carbons [357] and graphene [358] to obtain electrode materials with improved electrochemical performance. Amongst these, graphene possesses extraordinary properties like high specific surface area, high electrical conductivity, mechanical and thermal stability and can significantly boost the nanocomposite electrode performance as conductive filler. High specific surface area and porosity are essential parameters that increase the electrochemically active sites of the electrode thereby enhancing the ion adsorption and redox reaction rate [359, 360]. Several different methods have been explored to modify the electrode surface in order to achieve improved capacitive performance such as chemical activation [361], surface functionalization [362], covalent grafting [363], introducing surfactants [364], γ-irradiation [365] and swift heavy ion irradiation [366].

Swift heavy ion (SHI) irradiation has emerged as an effective technique in recent years for controlled modification of the surfaces and properties of materials at the atomic level. Different ion beams with varying energies and fluences have been used to tune the structure, morphology, optical, electrical and sensing properties of materials for a wide range of applications [367, 368]. Interaction of energetic ion beams with materials is governed mainly by two independent processes, (i) nuclear energy loss, which is caused by elastic collisions with the nuclei and dominates at low energy of ≈1 keV/amu, and (ii) electronic energy loss triggered by inelastic collisions of the projectile ions leading to excitation and ionization of the target atoms, which dominates at high energy of 1 MeV/amu or more [200]. The energy transfer mechanism has been explained by the coulomb explosion and thermal spike models as described in section 2.11 of Chapter 2 [203]. For SHI, the energy transfer occurs mainly by electronic energy loss that ranges from tens of eV to a few keV/Å. With this large amount of energy deposition in each collision, SHI becomes a unique tool over other methods for producing exotic and diverse effects in the target

material such as defect annealing, cluster of point defects, carbonization and formation of ion tracks. Conducting polymers, in particular, has been reported to undergo significant changes like chain scissioning, cross-linking, molecular fragmentation and formation of new chemical bonds with stimulated emission of gases that lead to different changes in their properties like density, conductivity, solubility etc. [206]. These changes are governed by the parameters of ion beam like ion mass and energy, fluence and the target material.

This chapter describes the swift heavy ion irradiation effects on the properties of reduced graphene oxide-polyaniline nanotubes (RGO-PAniNTs) nanocomposite with 40 wt. % of RGO concentration that showed the highest electrochemical performance as discussed in Chapter 6. The RGO-PAniNTs nanocomposite with 40 wt. % of RGO has been irradiated with 85 MeV C^{6+} SHI at four different ion fluences of 6×10^{10}, 3.6×10^{11}, 2.2×10^{12} and 1.3×10^{13} ions cm^{-2}. The detailed procedure of SHI irradiation has been discussed in section 3.5 of Chapter 3. The fluence dependent modifications in the morphology and chemical structure of the nanocomposite upon SHI irradiation have been studied by HRTEM, XRD, FTIR and micro-Raman spectroscopy. Thermogravimetric analysis, two-probe I-V and four-probe conductivity measurements have been carried out to study the thermal stability and electrical properties of the pristine (unirradiated) and irradiated nanocomposites. The surface properties and porosity of the nanocomposite before and after irradiation have been investigated by contact angle measurements and BET analysis. The electrochemical performance parameters of the pristine and irradiated nanocomposites at different fluences have been evaluated using cyclic voltammetry, galvanostatic charge-discharge and electrochemical impedance spectroscopy. The electrochemical stability of the pristine and irradiated nanocomposite electrodes has been determined for 1000 cycles.

7.2 Structural characterization

7.2.1 Morphological analysis

The effect of SHI irradiation with different fluences on the morphology of 40 wt. % RGO-PAniNTs nanocomposite has been studied by HRTEM and shown in Figure 7.1.

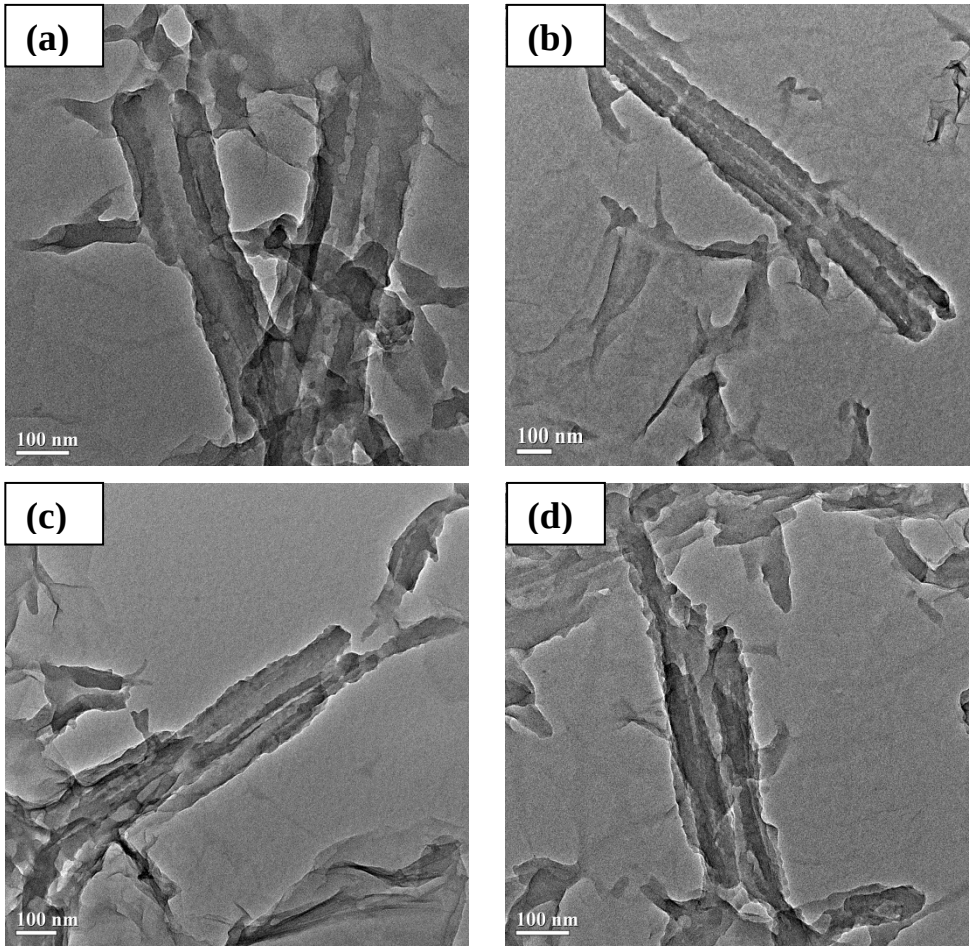

Figure 7.1: *HRTEM micrographs of 40 wt. % RGO-PAniNTs nanocomposites (a) pristine, and irradiated with fluence of (b) 6 × 10^{10}, (c) 2.2 × 10^{12} and (d) 1.3 × 10^{13} ions cm^{-2}.*

The HRTEM image of the pristine nanocomposite displays both RGO and PAniNTs indicating formation of the nanocomposite, where the average outer diameter of PAniNTs is measured to be about 134 nm. Upon irradiation, no change is visible in the morphology of RGO from HRTEM micrographs of the nanocomposites. On the other hand, PAniNTs undergo significant changes upon irradiation except for the nanocomposite irradiated with the lowest ion fluence of 6 × 10^{10} ions cm^{-2} [Figure 7.1 (b)] that appears to be similar with that of the pristine nanocomposite [Figure 7.1 (a)]. With increase in the fluence to 2.2 × 10^{12} ions cm^{-2}, broken portions of PAniNTs could be observed that indicates SHI induced fragmentation; however the outer boundary and the inner hollow core are not highly distorted. At the highest fluence of 1.3 × 10^{13} ions cm^{-2}, severe damage of PAniNTs occurs with indistinguishable inner hollow tube and outer surface indicating highly distorted

structure. The PAniNTs are highly degraded and shortened, however the diameter of the nanotubes does not decrease as observed in case of PPyNTs upon SHI irradiation. It appears that the inner hollow tubes are stable enough under SHI irradiation till a fluence of 2.2×10^{12} ions cm^{-2}, after which they are damaged resulting in complete destruction of PAniNTs.

7.2.2 X-ray diffraction analysis

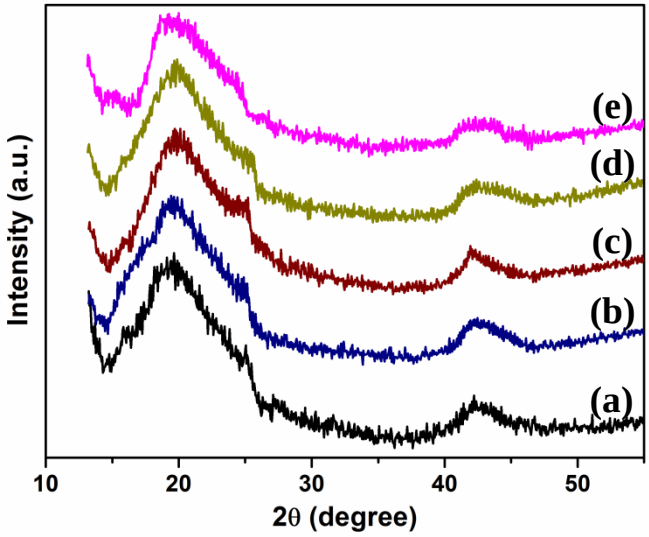

Figure 7.2: *X-ray diffractograms of 40 wt. % RGO-PAniNTs nanocomposites (a) pristine, and irradiated with fluence of (b) 6×10^{10}, (c) 3.6×10^{11}, (d) 2.2×10^{12} and (e) 1.3×10^{13} ions cm^{-2}.*

The XRD patterns of pristine and irradiated 40 wt. % RGO-PAniNTs nanocomposites are presented in Figure 7.2. Two broad peaks appear for pristine RGO-PAniNTs nanocomposite, one ranging from $2\theta = 15°$-$28°$ and the other centered at $2\theta = 43°$. The first peak arises due to overlapping of the peak of RGO at 24.6° and PAniNTs at 19.4° and 25°, respectively. The other broad peak at 43° is attributed to the (100) plane of graphite-like structure exhibited by RGO. The XRD patterns of the irradiated nanocomposites have similar diffraction peaks as compared to that of the pristine nanocomposite, indicating that no new phase has been formed on the surface of the nanocomposite after irradiation. The relative crystallinity percentage (X_C) of the nanocomposites has been evaluated from equation (3.7). The values of X_C of the pristine and irradiated nanocomposites with fluences of 6×10^{10}, 3.6×10^{11}, 2.2×10^{12} and 1.3×10^{13} ions cm^{-2} are found to be 42.6, 42.3, 42.5, 42.1

and 34.2%, respectively. The crystallinity of the nanocomposite is observed to be unaffected by SHI irradiation upto a fluence of 2.2×10^{12} ions cm^{-2}, after which a sharp decrease in crystallinity occurs. The decline in crystallinity at a fluence of 1.3×10^{13} ions cm^{-2} is due to chain scissioning of the polymer chains leading to fragmentation of PAniNTs by SHI at this fluence as evident from HRTEM micrographs. When energetic SHI passes through the nanocomposite film, bonds break and fragmentation starts occurring along the ion track core as the fluence crosses a threshold value [369] and the degree of fragmentation increases with further increase in fluence. However, amorphization of the material does not take place until the cylindrical damaged regions along the ion track core do not overlap. In the present case, the unaffected crystallinity upto a fluence of 2.2×10^{12} ions cm^{-2} indicates that the damaged regions do not overlap till that fluence, beyond which overlapping occurs leading to primary amorphization and decrease in crystallinity.

7.3 Vibrational spectroscopy

7.3.1 Fourier transform infrared spectroscopy

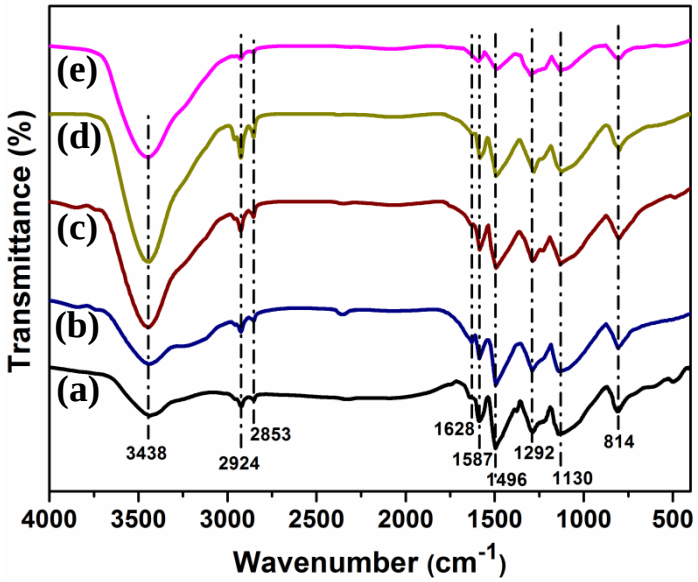

Figure 7.3: *FTIR spectra of 40 wt. % RGO-PAniNTs nanocomposites (a) pristine, and irradiated with fluence of (b) 6×10^{10}, (c) 3.6×10^{11}, (d) 2.2×10^{12} and (e) 1.3×10^{13} ions cm^{-2}.*

The FTIR spectra of the pristine and irradiated 40 wt. % RGO-PAniNTs nanocomposites are presented in Figure 7.3. The FTIR spectrum of the pristine

nanocomposite exhibits characteristic absorption bands of PAniNTs at 814, 1130, 1292, 1496 and 1587 cm^{-1}. The bands at 1496 and 1587 cm^{-1} are attributed to the C=C stretching vibration in benzenoid and quinoid rings of PAniNTs as discussed in Chapter 6. These characteristic bands of PAni are observed to weaken upon irradiation at the highest fluence of 1.3×10^{13} ions cm^{-2}, which is ascribed to breaking of bonds of PAni backbone chain upon irradiation. Absorption at 1130 and 1292 cm^{-1} corresponds to C-H in-plane bending and C-N stretching vibration of secondary aromatic amine, respectively [337, 336]. The C-H out-of-plane deformation of PAni is observed at 814 cm^{-1} [338]. The intensity of C-H in-plane bending and C-H out-of-plane deformation decreases at the highest fluence of irradiation. The small absorption peak at 1628 cm^{-1} for the pristine nanocomposite represents the C=C stretching vibration of sp^2 bonds of RGO [283]. This peak is observed to intensify upon irradiation at the fluence of 6×10^{10} ions cm^{-2}, which decreases upon further increase in fluence and completely disappear at the highest fluence. The absorption of CH and CH_2 groups at 2853 and 2924 cm^{-1}, respectively are observed both in the pristine and irradiated nanocomposites [340]. Absorption of O-H stretching vibrations appears as a broad peak centred at around 3438 cm^{-1} in both pristine and irradiated nanocomposites [339]. Table 7.1 presents the IR bands of 40 wt. % RGO-PAniNTs nanocomposite along with their respective peak positions.

Table 7.1: *Characteristic IR bands of 40 wt. % RGO-PAniNTs nanocomposite and their assignments*

IR Bands	**Assignments**
814 cm^{-1}	C-H out-of-plane deformation [338]
1130 cm^{-1}	C-H in-plane bending [337]
1292 cm^{-1}	C-N stretching [336]
1496, 1587 cm^{-1}	C=C stretching in benzenoid and quinoid rings of PAni [335]
1628 cm^{-1}	C=C stretching of RGO [283]
2853, 2924 cm^{-1}	CH and CH_2 stretching [340]
3438 cm^{-1}	O-H stretching [339]

7.3.2 Micro-Raman spectroscopy

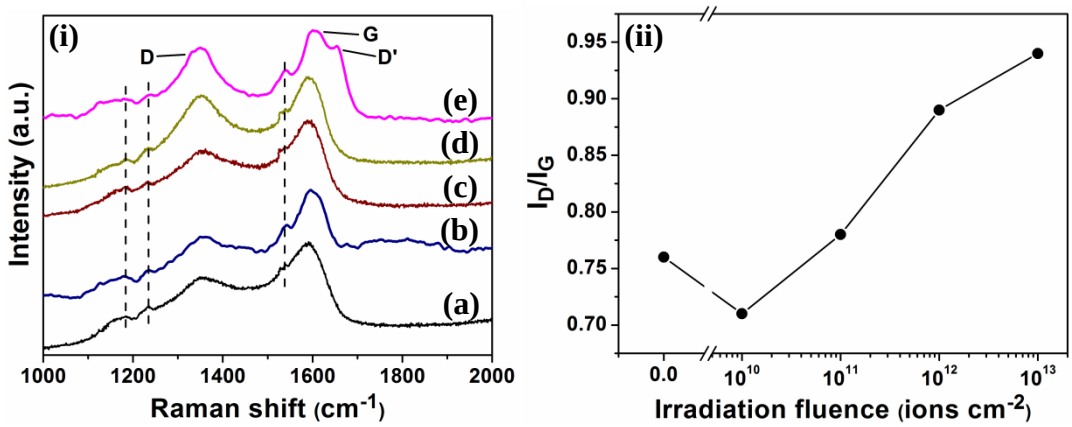

Figure 7.4: *(i) Micro-Raman spectra of 40 wt. % RGO-PAniNTs nanocomposites (a) pristine, and irradiated with fluence of (b) 6 × 10^{10}, (c) 3.6 × 10^{11}, (d) 2.2 × 10^{12} and (e) 1.3 × 10^{13} ions cm^{-2}; (ii) Variation of disorder parameter (I_D/I_G) with irradiation fluence.*

Micro-Raman spectroscopy has been performed to evaluate the defect density induced in 40 wt. % RGO-PAniNTs nanocomposite by SHI at different fluences and are shown in Figure 7.4 (i). The μ-Raman spectra of the pristine and irradiated nanocomposites show peaks at 1180, 1233, 1355, 1544 and 1595 cm^{-1}. The bands at 1180, 1233 and 1544 cm^{-1} arise from PAniNTs that correspond to the C-H bending of the quinoid or benzenoid ring, C-N stretching of benzene-diamine units and C=C stretching mode of the quinoid ring, respectively [370]. Two more peaks of PAniNTs attributed to the $C\text{-}N^{+}$ stretching of the bipolaron structure at 1350 cm^{-1} and C-C stretching of the benzenoid ring at 1608 cm^{-1} [343, 344] are observed to overlap with the D and G bands of RGO at 1355 and 1595 cm^{-1}, respectively. The most prominent bands observed in the μ-Raman spectra are the D and G bands. The G band appears due to in-plane vibration of sp^2 carbon atoms and the D band arises from a ring breathing mode of sp^2 atoms, which is activated only in the presence of structural imperfections and defects in a carbon material [371]. The ratio of intensities of the D and G bands (I_D/I_G), termed as the disorder parameter, provides information about defects density in a carbon nanostructure and can determine the ion irradiation induced damage in both RGO and PAniNTs [372, 319]. The disorder parameter is plotted against the irradiation fluence to study the SHI induced structural defects and is shown in Figure 7.4 (ii). Upon irradiation, the disorder

parameter is lowered at an initial fluence of 6×10^{10} ions cm^{-2} from 0.76 to 0.71 as compared to that of the pristine nanocomposite, which indicates less disorder and is a signature of annealing or re-arrangement of carbon atoms at moderate temperatures generated by the electronic energy deposition [320]. The re-arrangement of carbon atoms is corroborated by the intensified C=C stretching vibration of RGO at this fluence from FTIR spectra. On further increase in fluence, the disorder parameter increases to 0.78, 0.89 and 0.94 at fluences of 3.6×10^{11}, 2.2×10^{12} and 1.3×10^{13} ions cm^{-2}, respectively. This implies that SHI no longer anneal the defects beyond a certain fluence and results in growth of defects and distortions in the nanocomposite. This occurs as the electronic energy loss required for defect creation starts dominating over that required for defect annealing in the target material. The passage of SHI through the target material creates a highly ionized cylindrical zone of positive ions within a time period of 10^{-12} s due to the SHI induced excitation. As the mobility of the conduction electrons in the material is low enough to neutralize the charged cylindrical zone within a time interval of 10^{-12} s, it explodes radially under Coulomb repulsive forces [203]. This results in the generation of cylindrical shock waves through the target material leading to the formation of various types of defects such as point and columnar defects upto a continuous amorphized zone. Therefore, a maximum value of I_D/I_G = 0.94 at the dose of 1.3×10^{13} ions cm^{-2} indicates a dramatic increase in defects and structural disorder in the nanocomposite leading to amorphous transformation, which results in the appearance of another defect induced band D′ at 1621 cm^{-1} caused by an intra-valley double resonance process [318]. The obtained results corroborate with the sharp crystallinity decrease in the XRD pattern and the completely degraded PAniNTs evident from HRTEM at the highest fluence. The characteristic micro-Raman peaks of 40 wt. % RGO-PAniNTs nanocomposite with their corresponding peak positions have been assigned in Table 7.2.

Table 7.2: *Characteristic micro-Raman bands of 40 wt. % RGO-PAniNTs nanocomposite and their assignments*

Raman Bands	**Assignments**
1180 cm^{-1}	C-H bending of quinoid or benzenoid ring [342, 370]
1233 cm^{-1}	C-N stretching of benzene-diamine units [343, 370]
1355 cm^{-1}	D band: breathing mode from sp^2 carbon rings [371]

1544 cm^{-1}	C=C stretching of quinoid ring [344, 370]
1595 cm^{-1}	G band: in-plane sp^2 C-C stretching [371]
1621 cm^{-1}	D' band: arise due to double resonance intra-valley process in presence of defects [318]

7.4 Thermogravimetric analysis

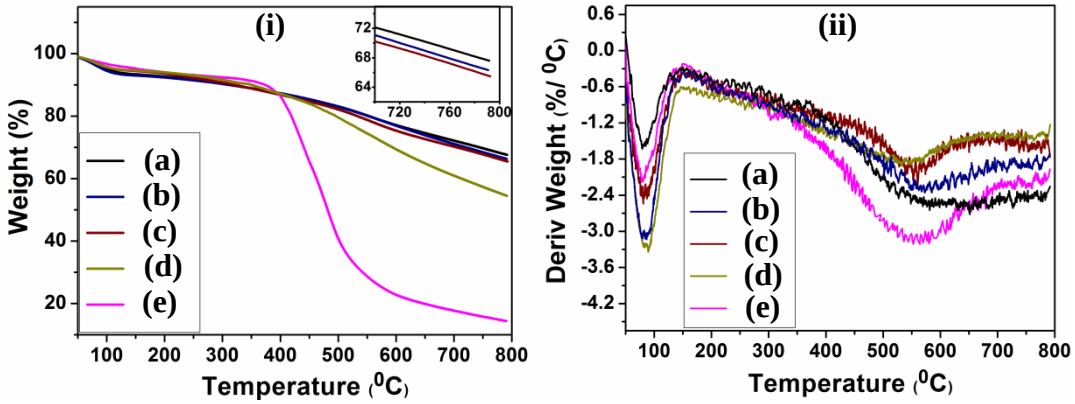

Figure 7.5: *(i) TG curves (Inset shows magnified TG curves) and (ii) derivative of TG curves of 40 wt. % RGO-PAniNTs nanocomposites (a) pristine, and irradiated with fluence of (b) 6 × 10^{10}, (c) 3.6 × 10^{11}, (d) 2.2 × 10^{12} and (e) 1.3 × 10^{13} ions cm^{-2}.*

The effect of SHI irradiation on the thermal properties of 40 wt. % RGO-PAniNTs nanocomposite at different fluences has been investigated by thermogravimetric analyzer in the temperature range of 50-800 °C and shown in Figure 7.5 (i). All the thermograms represent a two-step weight loss, the first one is observed in the range of 50-110 °C that corresponds to the evaporation of residual moisture. The second decomposition in the range of 370-800 °C is attributed to the thermal breakdown of PAni backbone as RGO being thermally stable does not show weight loss within this temperature range. The nanocomposite upon irradiation exhibit a slight increase in weight loss from 32% of that of pristine nanocomposite to 45% at an irradiation fluence of 2.2 × 10^{12} ions cm^{-2}, indicating an increase in degradation rate. However, a rapid decomposition of 85% occurs with increase in the fluence to 1.3 × 10^{13} ions cm^{-2}, which could be ascribed to the scissioning of the PAni backbone chain due to the energetic SHI bombardment.

The degradation mechanisms have been further studied from the derivative TG curves in terms of onset (T_{onset}) and rapidest decomposition temperatures (T_{rpd}) for the second degradation and the values are summarized in Table 7.3. The T_{onset} and T_{rpd} correspond to the temperature of the starting point of decomposition and the maximum decomposition. As shown in Figure 7.5 (ii), two peaks are observed in the derivative TG curves for all the nanocomposites that are attributed to the degradation of residual moisture and the main chain of PAni. With increasing fluence, both the T_{onset} and T_{rpd} are observed to decrease indicating thermal degradation of the nanocomposite upon irradiation. The lowest values of T_{onset} and T_{rpd} of 364 °C and 549 °C are observed for the 1.3×10^{13} ions cm^{-2} irradiated nanocomposite implying a dramatic decrease in thermal stability as evident from the broad derivative peak of the nanocomposite. The reduction in thermal stability at the highest irradiation fluence is attributed to multiple fragmentations and destruction of bonds due to overlapping of cylindrical ion tracks, which is consistent with the HRTEM results. Thus, the thermal degradation of 40 wt. % RGO-PAniNTs nanocomposite upon SHI irradiation is low till a fluence of 2.2×10^{12} ions cm^{-2} followed by a rapid weight loss at the highest fluence of 1.3×10^{13} ions cm^{-2}.

Table 7.3: *T_{onset}, T_{rpd} and and % of degradation at 800 °C of pristine and irradiated 40 wt. % RGO-PAniNTs nanocomposites with different fluences*

Sample	T_{onset} (°C)	T_{rpd} (°C)	Degradation at 800 °C (%)
Pristine	392	586	32.39
6×10^{10}	392	571	33.65
3.6×10^{11}	392	557	34.55
2.2×10^{12}	364	551	45.51
1.3×10^{13}	364	549	85.54

7.5 Current-voltage (I-V) characteristics

The room temperature I-V characteristics of pristine and irradiated 40 wt. % RGO-PAniNTs nanocomposites in the voltage range of -5 V to 5 V are shown in Figure 7.6 (i). The pristine as well as the irradiated nanocomposites exhibit a non-linear and symmetric variation of current with applied voltage. The non-linear I-V characteristics arise due to the inhomogeneous structure of the nanocomposite

consisting of conducting RGO nanosheets in a relatively less conducting PAni matrix. The I-V curves of the irradiated nanocomposites are observed to be similar to that of the pristine nanocomposite indicating same charge transport process of hopping after irradiation. The non-linear behavior of the I-V curves can be quantitatively analyzed by the Kaiser model according to which the conductance is given by following equation:

$$G = \frac{I}{V} = \frac{G_0 \, exp(^{V}/_{V_0})}{1 + h[exp(^{V}/_{V_0}) - 1]} \tag{7.1}$$

where G_0 is the temperature-dependent low-field conductance (for $V \rightarrow 0$), V_0 is the voltage scale factor that gives an exponential increase in conductance with increase in V and $h = {}^{G_0}/_{G_h}$ (where $h < 1$) yields a decrease in the G value below the exponential increase at higher voltages V. Due to symmetric nature of the I-V curves, the positive sides are considered for fitting according to equation (7.1) and are shown in Figure 7.6 (ii). The fitting parameters are presented in Table 7.4. It is noticed that an increase in the irradiation fluence till 2.2 × 10^{12} ions cm^{-2} causes an increase in the values of G_0, V_0 and h, which implies decrease in non-linearity of the I-V curves upon irradiation [224]. The decreased non-linearity indicates reduced tunnelling barriers between conductive regions for charge carrier hopping resulting in enhanced current in I-V characteristics.

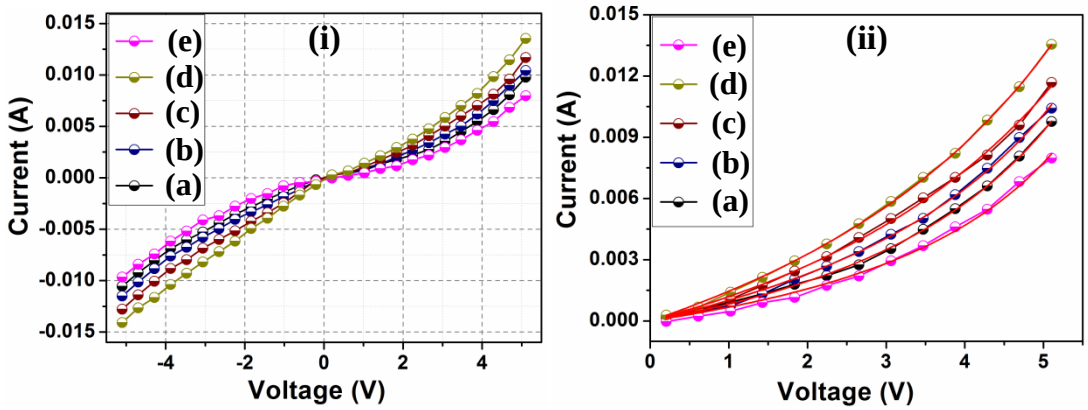

Figure 7.6: *(i) I-V characteristics and (ii) Kaiser equation fitted I-V curves of 40 wt. % RGO-PAniNTs nanocomposites (a) pristine, and irradiated with fluence of (b) 6 × 10^{10}, (c) 3.6 × 10^{11}, (d) 2.2 × 10^{12} and (e) 1.3 × 10^{13} ions cm^{-2}.*

Table 7.4: *Fitting parameters to Kaiser equation for pristine and irradiated 40 wt. % RGO-PAniNTs nanocomposites with different fluences*

Sample	G_0(S)	V_0 (V)	h
Pristine	9.71×10^{-4}	3.93	0.91
6×10^{10}	1.51×10^{-3}	4.09	0.91
3.6×10^{11}	1.66×10^{-3}	4.22	0.93
2.2×10^{12}	2.92×10^{-3}	4.36	0.95
1.3×10^{13}	6.91×10^{-4}	2.82	0.90

7.6 Conductivity measurements

The electrical conductivities of pristine and irradiated 40 wt. % RGO-PAniNTs nanocomposites are calculated at room temperature with four-probe method using equation (2.26). The average dc conductivities of pristine and irradiated nanocomposites with ion fluences of 6×10^{10}, 3.6×10^{11}, 2.2×10^{12} and 1.3×10^{13} ions cm^{-2} are found to be 8.04, 8.17, 8.46, 9.63 and 6.32 S cm^{-1}, respectively. The nanocomposite upon irradiation exhibit a slightly higher conductivity upto a fluence of 2.2×10^{12} ions cm^{-2} followed by a rapid drop in conductivity at the highest ion dose of 1.3×10^{13} ions cm^{-2}. The improved conductivity till a fluence of 2.2×10^{12} ions cm^{-2} could be ascribed to the generation of additional charge carriers and hopping sites for charge delocalization in the nanocomposite due to breaking of side-bonds upon irradiation [373]. The conductivity increase may also be accounted for the removal of oxygen containing groups from RGO due to the high electronic energy deposition of SHI leading to the restoration of delocalized sp^2 conjugated network. However, the conductivity decreases with increase in ion fluence to 1.3×10^{13} ions cm^{-2}, which may be due to the increased defect formation in RGO and completely degraded PAniNTs. Thus, it could be concluded that defect creation is not dominant enough till a fluence of 2.2×10^{12} ions cm^{-2}, after which the material becomes unstable to the incoming energetic ions leading to significant increase in defect sites resulting in the disruption of π-electron delocalization and decreased conductivity.

7.7 Surface area and pore size analysis

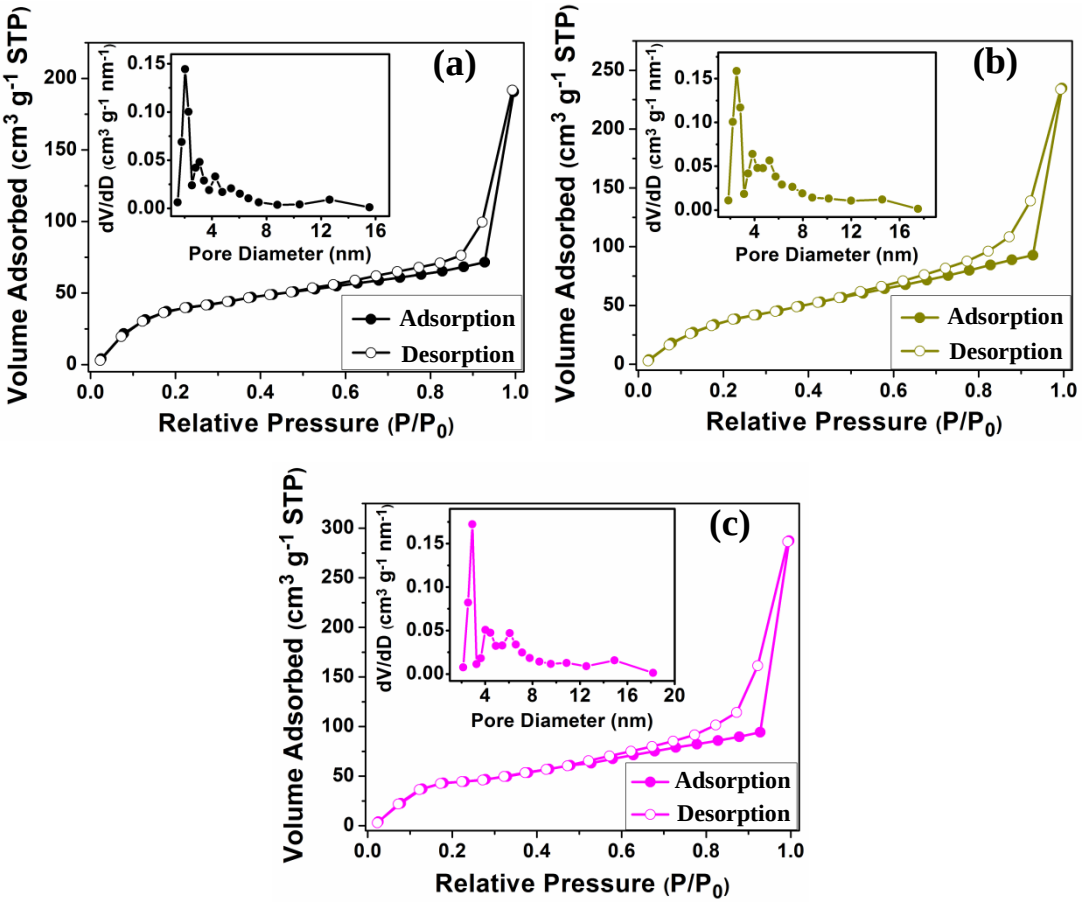

Figure 7.7: *N_2 adsorption-desorption isotherms of 40 wt. % RGO-PAniNTs nanocomposites (a) pristine, and irradiated with fluence of (b) 2.2 × 10^{12} and (c) 1.3 × 10^{13} ions cm^{-2}. The insets show the corresponding pore size distribution curves.*

To investigate the specific surface area and pore size distribution of 40 wt. % RGO-PAniNTs nanocomposite before and after SHI irradiation, N_2 adsorption-desorption measurements have been conducted and the isotherms are presented in Figure 7.7. The specific surface areas have been evaluated using the Brunauer-Emmett-Teller (BET) method from the adsorption branch in the relative pressure (P/P_0) range of 0.05-0.35. The BET results showed that the pristine RGO-PAniNTs nanocomposite exhibit a specific surface area of 196.08 m^2 g^{-1}. Upon irradiation, an increase in the specific surface area of the nanocomposite to 226.57 m^2 g^{-1} and 231.81 m^2 g^{-1} is obtained at a SHI irradiated fluence of 2.2 × 10^{12} ions cm^{-2} and 1.3 × 10^{13} ions cm^{-2}, respectively. The total pore volume is calculated from a single point adsorption at a relative pressure of 0.95 and is found to be 0.171 cm^3 g^{-1}, 0.214 cm^3 g^{-1} and 0.242

cm^3 g^{-1} for the pristine, 2.2 × 10^{12} ions cm^{-2} and 1.3 × 10^{13} ions cm^{-2} irradiated nanocomposites, respectively. The pore size distribution curves are obtained from the desorption branch using the Barrett-Joyner-Halenda (BJH) method and are shown in the insets of Figure 7.7. It is observed that the pore size of the pristine nanocomposite is in the range of 2-4 nm, which increases upon irradiation to 2-6 nm for the 2.2 × 10^{12} ions cm^{-2} and 1.3 × 10^{13} ions cm^{-2} irradiated nanocomposite indicating the presence of micropores in the nanocomposite films. The increase in specific surface area and porosity achieved upon irradiation could be ascribed to the SHI induced fragmentation of PAniNTs leading to shorter and higher surface area nanotubes as observed from HRTEM measurements.

7.8 Contact angle measurements

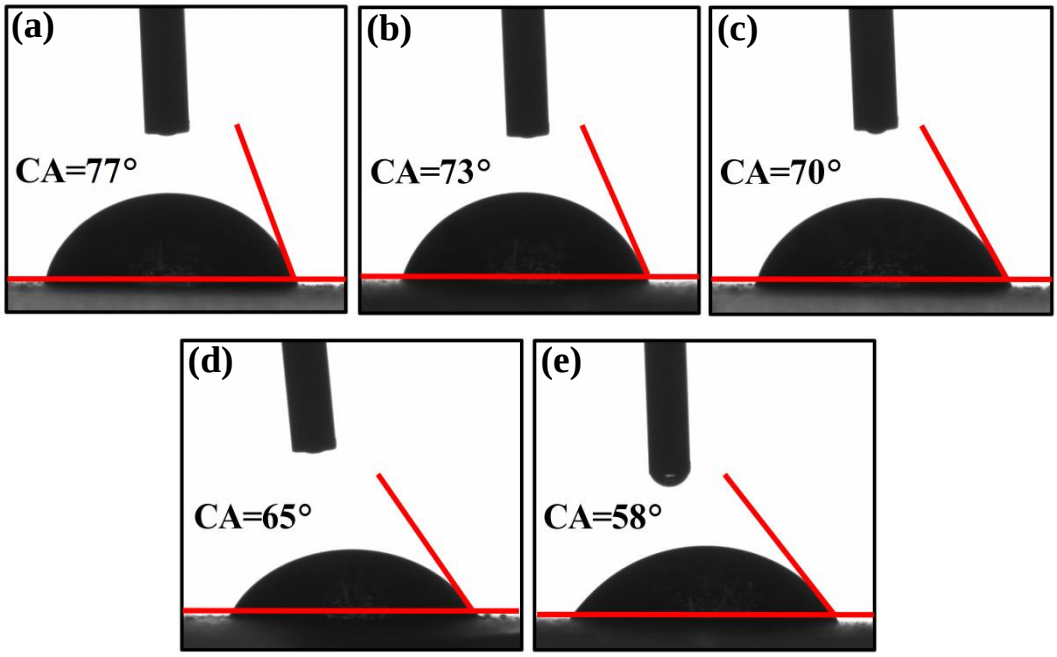

Figure 7.8: *Water contact angles of 40 wt. % RGO-PAniNTs nanocomposites (a) pristine, and irradiated with fluence of (b) 6 × 10^{10}, (c) 3.6 × 10^{11}, (d) 2.2 × 10^{12} and (e) 1.3 × 10^{13} ions cm^{-2}.*

Water contact angle measurements on pristine and irradiated 40 wt. % RGO-PAniNTs nanocomposite electrodes have been performed and presented in Figure 7.8. Pristine RGO-PAniNTs nanocomposite electrode exhibits a water contact angle of 77°. SHI irradiation of the nanocomposite results in a decrease in contact angle with increasing fluence. The lowest contact angles of 65° and 58° are obtained for

2.2×10^{12} and 1.3×10^{13} ions cm^{-2} irradiated nanocomposite electrodes. The significant decrease in contact angle of the nanocomposite electrode upon SHI irradiation indicates increased wettability of the electrode surface [374]. This implies that interaction of the electrode with the aqueous solvent increases after irradiation maximizing the electrolyte penetration into the electrode, which is beneficial for capacitive charge storage. As the surface wettability is related to the energy of the surface, the surface free energy of pristine and irradiated nanocomposite electrodes have been calculated to verify the increase in wettability using the Owens, Wendt, Rabel and Kaelble (OWRK) method. According to this method, the contact angles of two different liquids, one polar (water) and one apolar (diiodomethane) have been used for calculation of total surface energy in terms of polar and dispersive components according to equation (2.73). The measured contact angles of water and diiodomethane and the obtained values of total surface energy and its components for pristine and irradiated nanocomposite electrodes are listed in Table 7.5. It is observed that surface free energy of the nanocomposite electrode increases with increasing fluence of SHI irradiation. Therefore the water contact angle of the nanocomposite electrode decreases with increasing fluence due to the increase in surface free energy, implying improved wettability of the electrode surface. The improved wettability of the electrode surface may be attributed to the increase in specific surface area and porosity of the nanocomposite electrode upon irradiation as observed from N_2 adsorption-desorption measurements.

Table 7.5: *Contact angles of water and diiodomethane, values of total surface energy (Υ_s^{Total}) and its polar (Υ_s^p) and dispersive (Υ_s^d) components of pristine and irradiated 40 wt. % RGO-PAniNTs nanocomposites obtained by OWRK method*

Sample	Water	Diiodomethane	Υ_s^d	Υ_s^p	Υ_s^{Total} (mNm^{-1})
Pristine	77	63	26.84	8.15	34.99
6×10^{10}	73	59	29.15	9.34	38.49
3.6×10^{11}	70	56	30.87	10.29	41.16
2.2×10^{12}	65	52	33.15	12.15	45.30
1.3×10^{13}	58	47	35.92	13.05	48.97

7.9 Electrochemical properties

7.9.1 Cyclic voltammetry

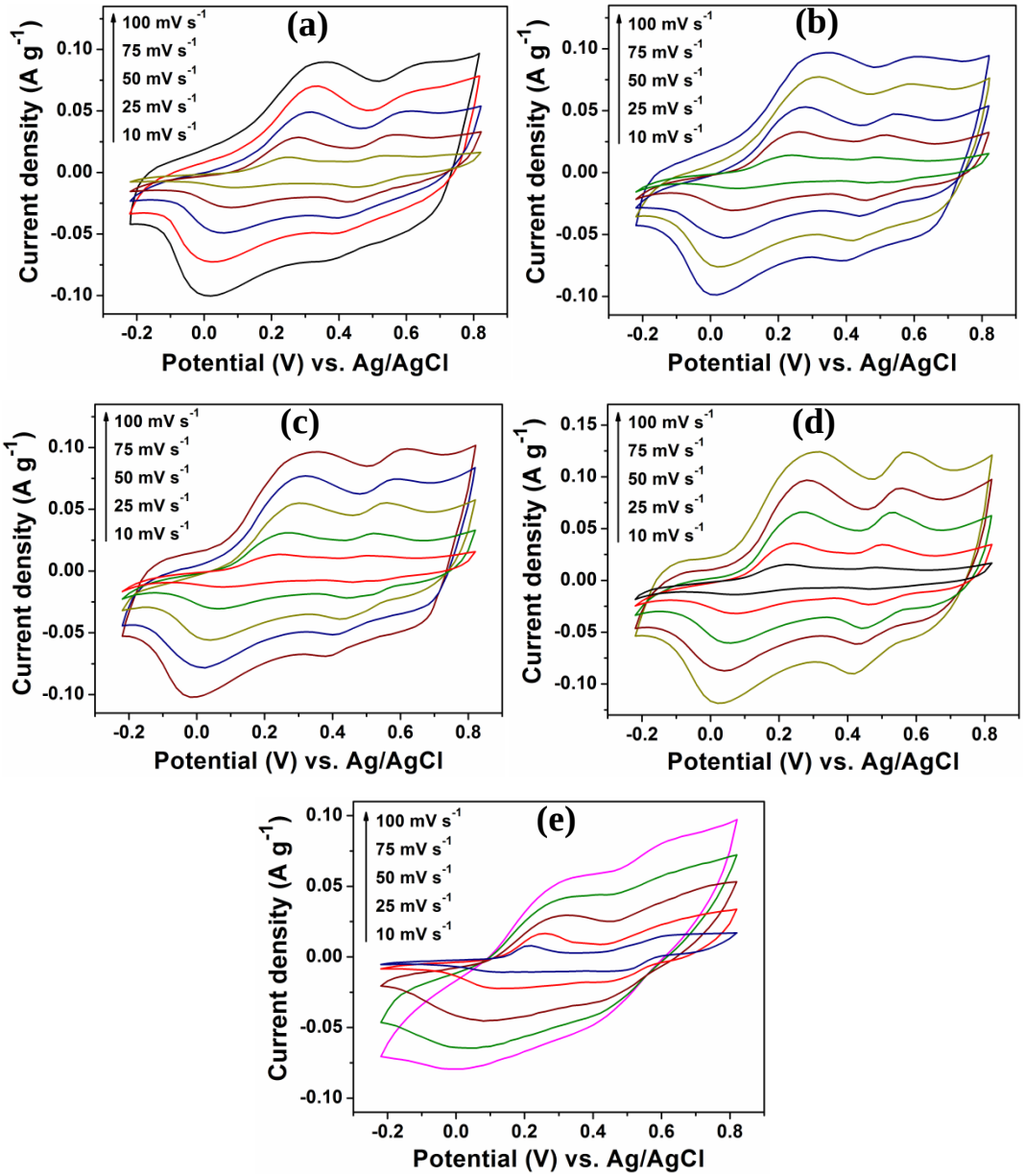

Figure 7.9: *CV curves at different voltage scan rate of 40 wt. % RGO-PAniNTs nanocomposites (a) pristine, and irradiated with fluence of (b) 6 × 10^{10}, (c) 3.6 × 10^{11}, (d) 2.2 × 10^{12} and (e) 1.3 × 10^{13} ions cm^{-2}.*

The CV curves of pristine and irradiated 40 wt. % RGO-PAniNTs nanocomposites have been recorded at different scan rates in 1 M H_2SO_4 electrolyte in the potential window of -0.2-0.8 V and shown in Figure 7.9. The CV curve of the pristine nanocomposite displays a quasi-rectangular shape with two distinct redox peaks

indicating that the charge storage mechanism in the electrode is a contribution of both EDLC and pseudocapacitance. The EDL behavior is exhibited by RGO and the pseudocapacitance originates from PAniNTs, where the two redox peaks are attributed to the leucoemeraldine-emeraldine and emeraldine-pernigraniline faradaic transitions of PAni, respectively [375]. Upon irradiation, it is observed that the current response and integral area of the CV curves increase with ion fluence upto 2.2×10^{12} ions cm^{-2}, followed by a drop at the highest fluence. The enhanced current response may result from the improved conductivity of the nanocomposite observed upto an ion fluence of 2.2×10^{12} ions cm^{-2} upon irradiation. Moreover, a change in the shape of the CV curves could be noted at different fluences of irradiation. Upon irradiation with a fluence of 6×10^{10} ions cm^{-2}, no significant change in the CV shape occurs. However, as the fluence increases to 3.6×10^{11} ions cm^{-2}, it is observed that the redox peaks become intense in the irradiated nanocomposite as compared to that of the pristine nanocomposite. With further increase in fluence, the intensity of the redox peaks increases and is most prominent at the fluence of 2.2×10^{12} ions cm^{-2} enclosing a larger integral area [Figure 7.9 (d)], beyond which complete disappearance of the peaks occur [Figure 7.9 (e)]. The change in the CV curve's shape could be attributed to the increase in surface area of the nanocomposite electrode upon irradiation as evident from BET analysis. The energetic SHI causes fragmentation in the nanocomposite electrode resulting in breaking and shortening of PAniNTs, which may increase the surface area of the electrode. The enhanced surface area increases the overall electrochemical active sites of PAniNTs leading to increased pseudocapacitive contribution, which results in intense redox peaks of PAni thereby improving the capacitive performance till a fluence of 2.2×10^{12} ions cm^{-2}. However, heavy irradiation at an ion fluence of 1.3×10^{13} ions cm^{-2} leads to severe damage of PAniNTs and it could no longer contribute to the faradaic redox reactions arising from its active sites resulting in complete absence of PAni redox peaks and diminished pseudocapacitance. Therefore, the integral area and current response of the CV curve decreases at the highest fluence and the CV curve exhibits a quasi-rectangular shape indicating EDLC as the dominant charge storage mechanism at that fluence.

7.9.2 Galvanostatic charge-discharge measurements

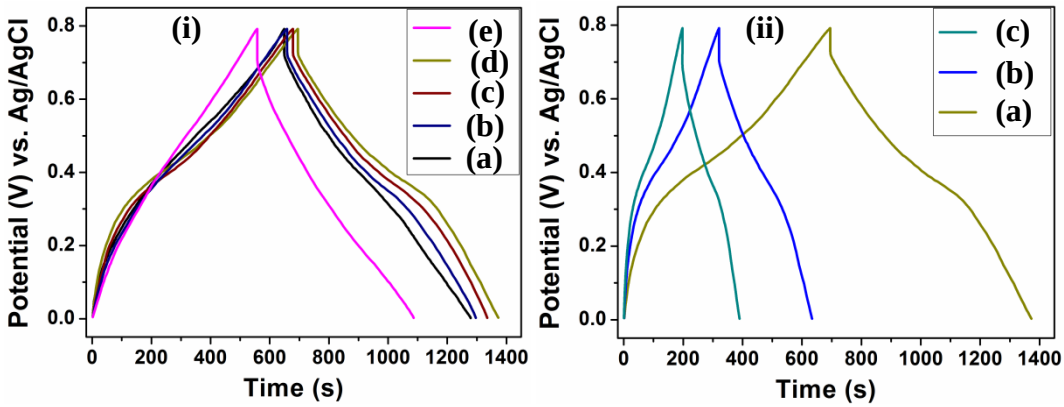

Figure 7.10: *(i) GCD curves of 40 wt. % RGO-PAniNTs nanocomposites (a) pristine, and irradiated with fluence of (b) 6 × 10^{10}, (c) 3.6 × 10^{11}, (d) 2.2 × 10^{12} and (e) 1.3 × 10^{13} ions cm^{-2} at a current density of 0.5 A g^{-1}; (ii) GCD curves of 2.2 × 10^{12} ions cm^{-2} irradiated RGO-PAniNTs nanocomposite at a current density of (a) 0.5 A g^{-1}, (b) 1 A g^{-1} and (c) 1.5 A g^{-1}.*

The GCD curves of pristine and irradiated 40 wt. % RGO-PAniNTs nanocomposites with different fluences at a current density of 0.5 A g^{-1} in the potential range of 0-0.8 V are shown in Figure 7.10 (i). The GCD curves of the pristine and irradiated nanocomposites upto a fluence of 2.2 × 10^{12} ions cm^{-2} reveal a linear discharge with a slight curvature indicating the presence of both EDL and pseudo capacitive features in the electrode. It is observed that SHI irradiation results in a longer discharge time of the nanocomposite electrode with increasing ion fluence upto 2.2 × 10^{12} ions cm^{-2} signifying improved charge storage and specific capacitance upon irradiation. The specific capacitances (C_{sp}) and the coulombic efficiency (η) of the pristine and irradiated nanocomposites have been evaluated from the GCD curves using equations (2.41) and (2.32) and are presented in Table 7.6. The highest specific capacitance and coulombic efficiency obtained after irradiation are 482 F g^{-1} and 97% at a fluence of 2.2 × 10^{12} ions cm^{-2} and its GCD curves with increasing current densities are displayed in Figure 7.10 (ii). The improved charge storage properties upon irradiation may be the consequence of enhanced surface area and porosity of the nanocomposite, which contributes to the available electroactive sites to be accessible by the electrolyte and facilitates the ion transport throughout the electrode. In addition, the presence of defects in a minimal amount induced by irradiation may

also give rise to improved capacitance. Defects can produce charged dangling bonds locally that are reactive towards adsorbates and can promote ion diffusion from the electrolyte to the electroactive surfaces [325]. However, this seems applicable till a fluence of 2.2×10^{12} ions cm^{-2}, after which the discharge duration and specific capacitance decrease. This could be attributed to the chain scissioning and structural breakdown of PAniNTs that limits its charge transfer reactions at the highest fluence of 1.3×10^{13} ions cm^{-2}, though an increase in surface area is observed from BET analysis. An increase in defect density of RGO at this fluence as observed from Raman measurements may also degrade the electrochemical performance. The values of energy density and power density are calculated using the following equations:

$$E(Wh/kg) = \frac{1}{2} C_{sp} (\Delta V)^2 \tag{7.2}$$

$$P(W/kg) = \frac{E}{\Delta t_d} \tag{7.3}$$

where C_{sp}, Δt_d and ΔV are the specific capacitance, discharge time and discharge potential, respectively. The calculated energy density and power density values are shown in Table 7.6. The highest energy density achieved is 32.81 W h kg^{-1} at a power density of 174.98 W kg^{-1} for the nanocomposite irradiated with SHI fluence of 2.2×10^{12} ions cm^{-2}.

Table 7.6: *Specific capacitance, energy density, power density, coulombic efficiency, equivalent series resistance (R_s) and charge transfer resistance (R_{ct}) of pristine and irradiated 40 wt. % RGO-PAniNTs nanocomposites with different fluences*

Sample	**Specific capacitance (F g^{-1})**	**Energy density (W h kg^{-1})**	**Power density (W kg^{-1})**	**Coulombic efficiency**	**R_s (Ω)**	**R_{ct} (Ω)**
Pristine	448.57	30.52	174.96	97%	5.29	4.05
6×10^{10}	456.42	31.01	174.70	97%	5.29	4.02
3.6×10^{11}	468.57	31.88	174.95	97%	5.25	3.95
2.2×10^{12}	482.14	32.81	174.98	97%	5.17	3.73
1.3×10^{13}	394.02	24.56	167.45	94%	5.33	4.61

7.9.3 Electrochemical impedance spectroscopy

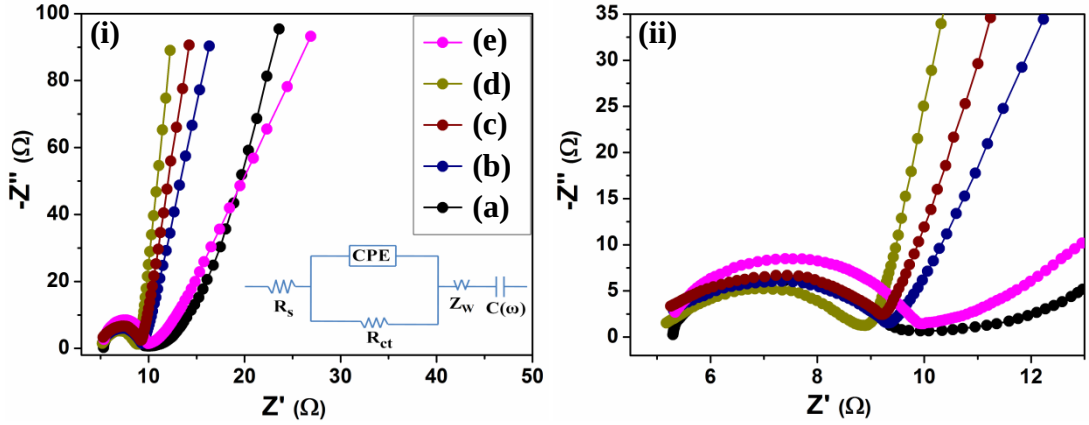

Figure 7.11: *(i) Nyquist plots of 40 wt. % RGO-PAniNTs nanocomposites (a) pristine, and irradiated with fluence of (b) 6 × 10^{10}, (c) 3.6 × 10^{11}, (d) 2.2 × 10^{12} and (e) 1.3 × 10^{13} ions cm^{-2} (Inset shows equivalent circuit) and (ii) Magnified view of the Nyquist plot in Z' range of 4.5-13 Ω.*

The electrochemical resistive processes of the pristine and irradiated 40 wt. % RGO-PAniNTs nanocomposite electrodes in the frequency range of 10 mHz to 50 kHz are studied by Nyquist plots as shown in Figure 7.11 (i). The plots consist of a semicircle at the high frequency region followed by a spike at low frequencies. The Nyquist plots have been analyzed using Randles equivalent circuit as shown in the inset of Figure 7.11 (i), which is comprised of equivalent series resistance (R_s), charge transfer resistance (R_{ct}) and interface resistance (CPE) in the high frequency range, while the low frequency region is governed by the Warburg impedance (Z_w) and supercapacitor cell capacitance (C(ω)), respectively [236]. The R_s and R_{ct} are evaluated from the magnified view of the Nyquist plots [Figure 7.11 (ii)] and presented in Table 7.6. The x-intercept of the Nyquist plot gives the R_s that include the ionic resistance of the electrolyte, intrinsic resistance of the active material and the contact resistance at the active material/current collector interface [376]. It is observed that SHI irradiation results in a slight decrease in R_s till an irradiation fluence of 2.2 × 10^{12} ions cm^{-2}, which might be ascribed to the improved conductivity of the electrode after irradiation. The R_{ct} is determined from the diameter of the semicircle, which is observed to decrease with increase in ion fluence upto 2.2 × 10^{12} ions cm^{-2}. This implies decreased resistance for charge transfer across the electrode/electrolyte interface as the SHI fluence increases, which may be

due to the higher surface area of the electrode providing additional active sites for faradaic reactions. The decreased Warburg impedance till a fluence of 2.2×10^{12} ions cm^{-2} represented by the 45° slope portion of the curve indicates easier diffusion of electrolyte ions into the electrode. Moreover, the increased linear shape of the impedance curve at low frequency with increasing irradiation fluence signifies improved capacitive behavior. However, all the resistances R_s, R_{ct} and Z_w increase as the ion fluence is increased to 1.3×10^{13} ions cm^{-2} revealing greater obstruction in ionic and electronic charge transport due to the SHI induced severe fragmentation and larger damaged areas at this fluence.

7.9.4 Cyclic stability study

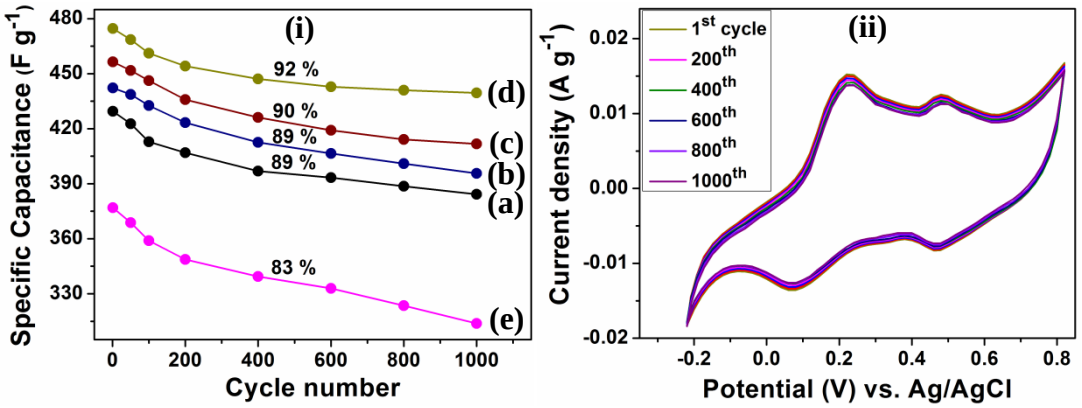

Figure 7.12: *(i) Variation of specific capacitance with cycle number of 40 wt. % RGO-PAniNTs nanocomposites (a) pristine, and irradiated with fluence of (b) 6×10^{10}, (c) 3.6×10^{11}, (d) 2.2×10^{12} and (e) 1.3×10^{13} ions cm^{-2}; (ii) CV curves with increasing cycle number of 40 wt. % RGO-PAniNTs nanocomposite irradiated at a fluence of 2.2×10^{12} ions cm^{-2}.*

The cyclic stability of an electrode is a significant parameter for application in supercapacitors. The cyclic stability of pristine and irradiated 40 wt. % RGO-PAniNTs nanocomposites has been evaluated for 1000 cycles by repeating the CV measurements at a scan rate of 10 mV s^{-1} in 1 M H_2SO_4 electrolyte. The specific capacitance values have been calculated with increasing CV cycles using equation (2.38) and are shown in Figure 7.12 (i). The capacitive retention of pristine nanocomposite is found to be 89% after 1000 consecutive cycles, which increases with increase in irradiation fluence. The highest capacitive retention with a

negligible capacitance loss of about 8% after 1000 cycles is recorded for the nanocomposite irradiated at an ion dose of 2.2×10^{12} ions cm^{-2}. Figure 7.12 (ii) shows the CV curves of the nanocomposite irradiated at a fluence of 2.2×10^{12} ions cm^{-2} with increasing cycle number upto 1000 cycles. It is observed that the shape of the CV curve suffers no significant change with increasing cycles indicating its improved electrochemical stability. This is possibly due to the increased surface area and electroactive sites for charge storage in the irradiated nanocomposites, which stabilize the capacitive performance with increasing cycle number. At the highest fluence of 1.3×10^{13} ions cm^{-2}, the cyclic stability drops to 83% that may be attributed to the increased concentration of defect sites and structural degradation due to high fluence of SHI irradiation.

7.10 Summary

RGO-PAniNTs nanocomposites with a RGO loading of 40 wt. % have been irradiated with 85 MeV C^{6+} swift heavy ions at four different fluences of 6×10^{10}, 3.6×10^{11}, 2.2×10^{12} and 1.3×10^{13} ions cm^{-2}. Morphological studies reveal fragmented and shortened PAniNTs without distortion of the tubular structure upto an ion fluence of 2.2×10^{12} ions cm^{-2} followed by highly distorted and degraded nanotubes at a higher fluence of 1.3×10^{13} ions cm^{-2}. X-ray diffractograms indicate a decrease in crystallinity of the nanocomposite from 42% for pristine nanocomposite to 34% for that irradiated at the highest fluence of 1.3×10^{13} ions cm^{-2}. In FTIR spectra, weakening of the bands associated with C=C stretching vibration in quinoid and benzenoid rings of PAniNTs occurs at the highest fluence of 1.3×10^{13} ions cm^{-2}, which indicates chain scissioning of backbone chain of PAniNTs due to large electronic energy deposition of SHI at this fluence. The disorder parameter evaluated from μ-Raman spectroscopy decreases first indicating re-arrangement of carbon atoms at a low fluence of 6×10^{10} ions cm^{-2} and then increases with further increase in ion fluence upto 1.3×10^{13} ions cm^{-2} due to SHI induced defects and disordered sites in the nanocomposite electrode. A decrease in thermal stability of the nanocomposite electrode is observed with increase in SHI irradiation fluence. However, a low degradation of 45% upto 800 °C is recorded upto a fluence of 2.2×10^{12} ions cm^{-2} as compared to 32% for that of the pristine nanocomposite, followed by fast degradation of 85% at the highest fluence of 1.3×10^{13} ions cm^{-2}. Derivative

TG curves display lower values of rapidest decomposition temperature with increase in SHI fluence indicating higher degradation rate of the nanocomposite upon irradiation. Current-voltage characteristics display an increase in current of the nanocomposite with increasing irradiation fluence till 2.2×10^{12} ions cm^{-2}. A small increase in conductivity is obtained from 8.04 S cm^{-1} for pristine nanocomposite to 9.63 S cm^{-1} for the nanocomposite irradiated at a fluence of 2.2×10^{12} ions cm^{-2}, which could be attributed to the generation of charge carriers and hopping sites for charge delocalization in the nanocomposite due to breaking of side-bonds upon irradiation. An increase in BET specific surface area of the nanocomposite occurs to 231 m^2 g^{-1} upon irradiation as compared to 196 m^2 g^{-1} for pristine nanocomposite. The pore size increases from 4 nm for pristine nanocomposite to 6 nm for 1.3×10^{13} ions cm^{-2} irradiated nanocomposite, which could be due to fragmentation and shortening of PAniNTs in the nanocomposite films upon irradiation leading to an increase in pore size and specific surface area. The enhanced specific surface area and porosity of the nanocomposites upon irradiation significantly improve the electrode wettability as observed from contact angle measurements. Upon irradiation, the CV curves of the nanocomposite exhibit enhanced integral area and PAni redox peaks. The intensity of the redox peaks increases and is maximum at the fluence of 2.2×10^{12} ions cm^{-2} encompassing a larger integral area, beyond which complete disappearance of the peak occur. This implies enhanced contribution of pseudocapacitance in the nanocomposite electrode upon irradiation upto a fluence of 2.2×10^{12} ions cm^{-2}. The absence of redox peaks at the highest fluence reveals reduced pseudocapacitance and dominant EDL charge storage in the nanocomposite electrode, which is due to severe damage of PAniNTs at a high fluence of 1.3×10^{13} ions cm^{-2}. GCD curves imply that SHI irradiation at fluence of 2.2×10^{12} ions cm^{-2} increases the specific capacitance of 40 wt. % RGO-PAniNTs nanocomposite to 482 F g^{-1} from 448 F g^{-1} for the pristine nanocomposite. A maximum energy density of 32 W h kg^{-1} is achieved at a power density of 174 W kg^{-1} for the nanocomposite irradiated with SHI fluence of 2.2×10^{12} ions cm^{-2}. The enhanced capacitive performance upon irradiation is attributed to increase in specific surface area and porosity of the nanocomposites, which provides more electrochemically active sites for charge storage. At the highest fluence of 1.3×10^{13} ions cm^{-2}, the capacitance decreases to 394 F g^{-1} due to increased structural degradation of PAniNTs at this fluence limiting its faradaic charge transfer reactions. The equivalent series

resistance and charge transfer resistance of the nanocomposite electrode decrease upon irradiation from 5.29 Ω to 5.17 Ω and 4.05 Ω to 3.73 Ω, respectively with increasing ion fluence upto 2.2×10^{12} ions cm^{-2}, beyond which severe damage of the nanocomposite induced by the high ion dose of 1.3×10^{13} ions cm^{-2} leads to an increased contact and interfacial resistances. Irradiation of the nanocomposite results in an increase in cyclic stability from 89% for pristine nanocomposite to 92% for 2.2×10^{12} ions cm^{-2} irradiated nanocomposite.